***Straightjacket/α2δ3* deregulation is associated with cardiac conduction defects in Myotonic Dystrophy type 1**

Emilie Plantié[1], Masayuki Nakamori[2], Yoan Renaud[3], Aline Huguet[4], Caroline Choquet5, Cristiana Dondi[1], Lucile Miquerol[5], Masanori Takahashi[6], Geneviève Gourdon[4], Guillaume Junion[1], Teresa Jagla[1], Monika Zmojdzian[1*] and Krzysztof Jagla[1*]

[1] *GReD, CNRS UMR6293, INSERM U1103, University of Clermont Auvergne, 28, Place Henri Dunant, 63000 Clermont-Ferrand, France*

[2] *Department of Neurology, Osaka University Graduate School of Medicine, 2-2 Yamadaoka, Suita, Osaka 565-0871, Japan*

[3] *BYONET (www.byonet.fr)*

[4] *Imagine Institute, Inserm UMR1163, 24, boulevard de Montparnasse, 75015 Paris, France*

[5] *Aix-Marseille University, CNRS UMR7288, IBDM Luminy Campus Case 907, 13288 Marseille cedex 9, France*

[6] *Department of Functional Diagnostic Science, Osaka University Graduate School of Medicine, 1-7 Yamadaoka, Suita, Osaka 565-0871, Japan*

- Correspondence to: Krzysztof Jagla christophe.jagla@uca.fr
  and Monika Zmojdzian monika.zmojdzian@uca.fr
  tel. +33 473178181; GReD, CNRS UMR6293, INSERM U1103, University of Clermont Auvergne, 28, Place Henri Dunant, 63000 Clermont-Ferrand, France

ABSTRACT

Cardiac conduction defects decrease life expectancy in myotonic dystrophy type 1 (DM1), a complex toxic CTG repeat disorder involving misbalance between two RNA-binding factors, MBNL1 and CELF1. How this pathogenic DM1 condition translates into cardiac conduction disorders remains unknown. Here, we simulated MBNL1 and CELF1 misbalance in the *Drosophila* heart and identified associated gene deregulations using transcriptional profiling of cardiac cells. We detected increased transcript levels of *straightjacket/α2δ3* that encodes a regulatory subunit of a voltage-gated calcium channel. *Straightjacket* overexpression in the fly heart leads to asynchronous heart beating that could result from affected conduction, whereas cardiac knockdown improves these symptoms. We also show that ventricular *α2δ3* expression is low in healthy mice and humans but significantly elevated in ventricular muscles from DM1 patients with conduction defects. Taken together, this suggests that keeping the *straightjacket/α2δ3* transcript levels low in ventricular cardiomyocytes could be a strategy to prevent conduction defects in DM1 pathology.

Key words: Myotonic Dystrophy type 1, *Drosophila*, heart, conduction defects, TU-tagging

SIGNIFICANCE

Cardiac conduction defects decrease life expectancy of patients suffering from DM1 but how DM1 condition translates into cardiac conduction disorders remains unknown. Here to identify gene deregulations underlying cardiac dysfunction in DM1, we used *Drosophila* model and TU-tagging-based heart-specific transcriptional profiling. We detected aberrant expression of several genes involved in cardiac Calcium handling and among them increased transcript levels of *straightjacket/α2δ3* that regulates calcium current density and triggers cardiac contractions. Because reducing expression of *stj* in cardiomyocytes of DM1 flies ameliorates asynchronous heart beating and ventricular *α2δ3* expression is significantly elevated in ventricular muscles from DM1 patients with conduction defects, we hypothesize that fine-tuning of *stj/α2δ3* expression could represent a way to treat DM1-associated cardiac pathology.

INTRODUCTION

Myotonic Dystrophy type 1 (DM1), the most prevalent muscular dystrophy found in adults [1], is caused by a CTG triplet repeat expansion in the 3' untranslated region of the *dystrophia myotonica protein kinase* (*dmpk*) gene. Transcripts of the mutated *dmpk*, containing expanded CUGs, form hairpin-like secondary structures in the nuclei, and sequester RNA-binding proteins with affinity to CUG-rich sequences. Among them, Muscleblind-like 1 (MBNL1) protein is trapped within the repeats, forming nuclear *foci* aggregates that hallmark the disease [2,3]. In parallel, the CUGBP- and ELAV-like family member 1 (CELF1) gets stabilized [4], creating misbalance between MBNL1 and CELF1. This leads to missplicing of several transcripts and a general shift from adult to fetal isoforms [5–7]. In addition, repeat toxicity induces a range of splice-independent alterations including affected transcript stability [8]. There is thus a combination of splice-dependent and splice-independent events underlying DM1 pathogenesis. DM1 targets mainly skeletal muscles and the heart, with about 80% of DM1 patients showing altered heart function with arrhythmia and conduction disturbance, which can eventually give rise to heart block and sudden death [9–11]. Consequently, cardiac symptoms, and particularly conduction defects, contribute to decreased life expectancy in DM1 [12].

To gain insight into mechanisms underlying cardiac dysfunction in DM1, we used *Drosophila* DM1 models, we had previously described [13]. The heart of the fruit fly, even if simple in structure, nevertheless displays just like the human heart, pacemaker-regulated rhythmic beating involving functions of conserved ion channels [14,15]. We simulated pathogenic MBNL1/CELF1 misbalance specifically in the fly heart by attenuating the *Drosophila MBNL1* ortholog *Muscleblind (Mbl*) and by overexpressing the *CELF1* counterpart *Bruno-3* (*Bru-3*) [16]. This led to asynchronous heartbeat (anterior and posterior heartbeats at a different rate) that in *Drosophila* could result from partial conduction block [17]. By using these two fly DM1 models, we hoped to identify molecular players involved in DM1-associated conduction and heart rhythm defects. In order to identify deregulated genes underlying this pathological condition, we applied a heart-targeted TU-tagging approach [18] followed by RNA sequencing. This cardiac cell-specific genome-wide approach yielded a discrete number of evolutionarily conserved candidate genes with altered cardiac expression in both DM1 models used. Among them, we found increased transcripts levels of *straightjacket* (*stj*)*/CACNA2D3 (α2δ3)*, which encodes a major regulatory subunit of Ca-α1D/Ca_v1.2 voltage-gated calcium channels, and is a key regulator of calcium current density

that triggers cardiac contraction [19–22]. The role of *stj* transcript level in proper conduction is supported by cardiac-specific overexpression of *stj* that leads to asynchronous heartbeat. Conversely, attenuating its expression by cardiac-specific knockdown in both DM1 fly heart models reverses cardiac asynchrony. Our hypothesis that *stj* is a possible mediator of the cardiac DM1-associated pathology is supported by our finding that ventricular *α2δ3* expression level is low in healthy mouse and human hearts, but is significantly increased in DM1 patients with cardiac conduction defects. This indicates that lowering *α2δ3* in ventricular cardiomyocytes could offer a potential treatment strategy for DM1-associated conduction defects.

RESULTS AND DISCUSSION

Imbalance of MBNL1 and CELF1 counterparts in the *Drosophila* heart results in asynchronous heartbeat

To mimic the DM1-associated imbalance between the RNA binding factors MBNL1 and CELF1 in *Drosophila*, we either knocked down the *MBNL1* ortholog, *Mbl*, or overexpressed the *CELF1* counterpart, *Bru-3*. We used the GAL4/UAS system with a cardiac-specific Gal4 driver line, *Hand-Gal4* to target UAS-driven transgene expression in the adult heart (**Fig. 1A**). We found that the *UAS-MblRNAi* line efficiently attenuates *Mbl* expression, whereas *UAS-Bru-3* generates *Bru-3* overexpression in GAL4-expressing cardiac cells (**Fig. S1**), both leading to asynchronous heartbeats, that could result from impulse propagation/conduction disturbance [17]. Moreover, the *Hand-Gal4* driven attenuation of *Mbl* and overexpression of *Bru-3,* both appear to be homogenous along the heart tube (**Fig. S1**).

First, we assessed Mbl and Bru-3 expression patterns in the adult fly and found that both proteins are present in the heart cells including contractile cardiomyocytes, and localize predominantly but not exclusively to the nuclei (**Fig. S1**). We then assessed the cardiac function in flies with attenuated *Mbl* or with *Bru-3* overexpression. To this end, we used the Semi-automated Optical Heartbeat Analysis (SOHA) method, which consists in filming the adult beating heart from hemi-dissected flies in order to analyze the contractile and rhythmic heart parameters [14,23]. In addition to frequently observed arrhythmia (e.g. **Fig. 1C**, A4 M-modes), about 58% of *Hand>MblRNAi* and 25% of *Hand>Bru-3* flies displayed asynchronous heartbeat, meaning the anterior and posterior heart segments had different beat rates **(Fig. 1B,C)**. The fact that reduction of heartbeat rate always follows impulse propagation direction supports the view that heart asynchrony is due to conduction defects [17], suggesting that, like in DM1 patients, an imbalance between MBNL1 and CELF1 in flies could also lead to conduction disturbances. In some cases, asynchronous heartbeat could result in total heart block when at least one heart segment stops contracting. Indeed, about 3% of *Hand>MblRNAi* and 10% of *Hand-Bru-3* flies developed a total heart block here (**Fig. 1C**).

Taken together, these data revealed that the imbalance of Mbl/MBNL1 and Bru-3/CELF1 in the heart leads to disruption of heart synchrony in flies, likely due to impulse propagation/conduction defects [17]. This prompted us to perform transcriptional profiling of

Hand>MblRNAi and *Hand>Bru-3* in cardiac cells to identify misregulated gene expression underlying this phenotype.

Transcriptional profiling of DM1 *Drosophila* models with heart asynchrony revealed increased levels of *straightjacket/α2δ3*, a conserved regulator of Ca^{2+} inward current

Transcriptional profiling of cardiac cells from *Hand>MblRNAi* and *Hand>Bru-3* flies was performed using a cell-specific approach called TU-tagging [18], followed by RNA-seq. This method allows tissue-specific RNA isolation by expressing uracil phosphoribosyltransferase (UPRT) enzyme in a cell-specific manner and incorporation into neo-synthesized transcripts of a modified Uracil, i.e. 4TU. Here, *Hand-GAL4*-driven UPRT expression in cardiac cells allowed us to isolate transcripts from adult heart cells only (**Fig. S2A**) and combining *UAS-UPRT* with *UAS-MblRNAi* and *UAS-Bru-3* lines to perform TU-tagging in our DM1 contexts (**Fig. S2A**, TU-tagging pipeline). Comparison of RNA-seq data from input RNA fraction and heart-specific TU-fraction from control *Hand>LacZ;UPRT* flies was used to assess suitability of TU-tagging in heart cells, which are in low abundance. We found that transcript levels of cardiac-specific genes such as *Hand* and *Tin* were highly enriched in the cardiac-tagged TU-fractions, whereas the transcript level of *Npc1b* and *Obp19b* genes expressed in midgut [24] and gustatory cells [25], respectively, were depleted (**Fig. S2A**, volcano graph and RNAseq tracks). Thus, the TU-tagging method turned out to be well suited for transcriptional profiling of adult *Drosophila* cardiac cells allowing to identify both global gene deregulations (analyzed here) as well as isoform-specific differential gene expression (representing a parallel study). To select candidates with a potential role in conduction disturbance, we focused on a pool of genes commonly deregulated in *Hand>MblRNAi* and in *Hand>Bru-3* contexts (**Fig. 2A**, Venn diagram). This pools counts 118 genes, including 64 conserved in humans (**Table S1** and **Fig. 2A**, heatmap), for which gene interaction network analysis (**Fig. 2A**, Genemania network) identified 4 candidates involved in the regulation of cellular Ca^{2+} level and known to be essential for proper cardiac conduction [26], i.e. *inactivation no afterpotential D* (*inaD*), *syntrophin-like 1* (*syn1*), *Rad, Gem/Kir family member 2* (*Rgk2*) and *straightjacket* (*stj*). Their respective human orthologs are *FRMPD2, SNTA1*, *REM1* and CACNA2D3/*α2δ3*. *inaD/FRMPD2* and *syn1/SNTA1* encode scaffolding PDZ domain proteins with regulatory functions on TRP Ca^{2+} channels [27,28] whose mutations cause cardiac hypertrophy, arrhythmia, and heart block [29]. Moreover, InaD was reported to prevent depletion of ER calcium store by inhibiting Ca^{2+}

release-activated Ca^{2+} (CRAC) channels [30]. Rgk2/REM1 belongs to the Ras superfamily of small GTP-binding proteins [31]. Rgk proteins, including Rgk2, interact with the α or β-subunit of $Ca_V1.2$ calcium channel and negatively regulate its function [31,32]. However, by interacting with CaMKII and with Rho kinase, both involved in cardiac hypertrophy and heart block Rgk proteins could also influence heartbeat in a Cav1.2 independent way. Finally, *stj/α2δ3* encodes auxiliary subunit of this same $Ca_V1.2$ channel, and is known to positively regulate this channel's abundance and consequently affects Ca^{2+} inward current [20]. *$Ca_V1.2$* mutations are known to lead to diverse heartbeat dysfunctions [33], and *$Ca_V1.2$* deregulation is associated with DM1 [34]. Importantly, the *Drosophila* counterpart of Cav1.2 (Ca-1αD) is also ensuring cardiac contractions and calcium transients in the fly heart [35] suggesting a conserved role of Cav1.2/ Ca-1αD in heart beating. Since mutations in *α2δ4,* and its paralog *α2δ3*, are associated with familial atrial fibrillation [36] and because *α2δ3* positively regulates Cav1.2 involved in DM1 [20,34], we wondered if altering expression of *stj/α2δ3* could contribute to DM1 cardiac defects. This was supported by the finding that *stj* transcript levels are significantly increased in both *Hand>MblRNAi* and in *Hand>Bru-3* contexts (**Fig. 2B,** RNA-seq tracks), whereas expression of two other *Drosophila α2δ* genes (*CG42817* and *CG16868)* remains unchanged (**Fig. S2B**). One potential mechanism of observed *stj* transcript elevation is the regulation of *stj* stability, a possibility supported by a selective increase of *stj-B* and *stj-C* isoforms carrying consensus Bru-3 and Mbl binding sites within their 3'UTRs region (**Fig. 2B**) and by the RIP experiment from dissected *Hand>Bru-3* hearts revealing that Bru-3 binds to this region (**Fig. 2C**). Similar to *α2δ* gene functions previously described [19], the higher *stj* level observed in our models could lead to increased Ca^{2+} inward current, thus affecting heartbeat heart parameters. Considering the high conservation of functional motifs and overall protein structure between human α2δ3 and *Drosophila* Stj (**Fig. 2D**), we hypothesize that the human α2δ3 could hold a similar function.

Increased cardiac expression of *stj/α2δ3* leads to asynchronous heartbeats in flies and is induced in ventricular cardiomyocytes of DM1 patients with conduction disturbance

To determine the cardiac function of Stj/α2δ3, we first tested whether these proteins indeed accumulate in adult fly and mouse hearts. A weak cytoplasmic Stj signal associated with circular myofibers of cardiomyocytes and a strong signal in the myofibers of ventral longitudinal muscle (VLM) underlying the heart tube [37] was visible in the adult *Drosophila*

heart (**Fig. 3A,** also see scheme **Fig. 3C**) stained with anti-Stj antibody [38]. In the VLM and in the heart-attaching alary muscles (AM), Stj expression resembled a T-tubule pattern. Like Stj, α2δ3 protein was also detected in the mouse heart (**Fig. 3B**), with high levels accumulating in the atrial cardiomyocytes. α2δ3 expression appeared low in the ventricular cardiomyocytes (**Fig. 3B),** similarly to Stj expression in the analogous fly heart tube cardiomyocytes. This differential α2δ3 expression in atria and ventricles was also seen at transcript levels (**Fig. 3B**, RT-qPCR graph). The role of *stj/α2δ3* potentially affecting the heartbeat patterns has not yet been investigated, but the fact that in healthy fly hearts and mouse ventricles it is expressed at low levels could have functional significance. To test this hypothesis, we took advantage of the fly model and overexpressed *stj* in the adult heart using *Hand-Gal4* and in cardiomyocytes only using *Tin-Gal4* (**Fig. 3E**). When driven with *Hand-Gal4* (**Fig. 3E)**, about 20% of individuals overexpressing *stj* displayed conduction defects, and the percentage of flies with asynchronous heartbeat increased to 30% in the *Tin>stj* context (**Fig. 3E**). This suggests that in flies, a high Stj level in cardiomyocytes creates a risk of conduction disturbance leading in some cases to total heart block (**Fig. 3E**, M-modes). We were however unable to test *α2δ3* involvement in cardiac conduction defects in mouse models of DM1 because the carrying large repeats number DMSXL mice [39] display only mild cardiac involvement without conduction disturbance.

As revealed by our heart-specific transcriptional profiling (**Fig. 2**), *rgk2* involved in Cav1.2/Ca-α1D regulation, could also contribute to heartbeat phenotypes in DM1. Indeed, a large portion of *Hand>Rgk2RNAi* flies showed total or partial heartbeat arrest (asystole) (**Fig. S3B**), increased arrhythmia and impaired contractility (**Fig. S3C**) but none developed asynchronous heartbeat (**Fig. S3D**). Consistent with recently reported data [35,40], heartbeat parameters have also been affected *in Hand>Ca-α1DRNAi* flies (**Fig. S3B,C**). Of note, about 18% of *Hand>Ca-α1DRNAi* flies showed asynchronous heartbeats indicating that to some extent, lowering *Ca-α1D* could also impact on heart synchrony. This observation prompted us to verify *Ca-α1D* transcript levels in our *Hand>Bru-3* and *Hand>MblRNAi* cardiac datasets. *Ca-α1D* has not been preselected among genes commonly deregulated in both DM1 contexts, however its transcript level appears specifically reduced in *Hand>MblRNAi* fly hearts compared to control (*Hand>lacZ*) and to *Hand>Bru-3* contexts (**Fig. S3A**), suggesting that this deregulation could contribute to heartbeat defects (including conduction defects) in *Hand>MblRNAi* flies. Moreover, *Ca-α1D* has numerous transcript isoforms but does not seem to be a target of Mbl and/or Bru-3 for alternative splice regulation (**Fig. S3A**).

To determine whether our data from the fly model could be relevant for DM1 patients, we used RT-qPCR to test *α2δ3* expression in ventricular cardiac muscle tissue from normal controls and from DM1 patients with conduction defects (**Fig. 3F**). Ventricular transcript levels of *α2δ3* were significantly higher (p=0.03) in DM1 patients with conduction defects, indicating a link between DM1, cardiac *α2δ3* transcript regulation and conduction disturbance.

Reducing *stj* transcript level in the heart partially rescues asynchronous heartbeats in *Drosophila* DM1 models

To make a link between calcium transient and heart asynchrony, we tested propagation of calcium waves in normal and in asynchronously beating hearts. We applied the GCaMP3 fluorescent calcium sensor that allows detection of calcium waves *in vivo* [35]. As shown in **Fig. 4A**, in wild type hearts, calcium waves underlie perfectly cardiac contractions so that each calcium peak aligns with the beginning of contraction along the heart tube (here registered in segments A3 and A4. In contrast, in asynchronously beating *Hand>MblRNAi* heart (**Fig. 4A**), in the anterior A3 segment, calcium peaks are not always in perfect alignment with contractions and appear not detectable in A4 segment that does not beat. Thus, these data show that calcium waves correlate with cardiac contractions in normal fly hearts and are affected in asynchronously beating hearts making the link between calcium current regulation and DM1-associated conduction defects.

To better assess the role of *stj* deregulation in pathogenic DM1 contexts, we attempted to correlate Stj protein expression level in *Hand>Bru-3, Hand>MblRNAi* and *Hand>stj* fly hearts with the extent of cardiac asynchrony in these contexts. We found that Stj signal in the cardiomyocytes was higher in *Hand>stj* flies than in *Hand>MblRNAi* and *Hand>Bru-3* flies (**Fig. S4**). However, the percentage of flies displaying conduction defects was higher in the *Hand>MblRNAi* context than the *Hand>stj* context (compare **Fig. 1B** and **Fig. 3E**). This thus suggests that Stj is not the sole factor whose deregulation causes asynchronous heartbeat in the *Hand>MblRNAi* context. To test whether *stj* is a required mediator of *Bru-3*-overexpression and/or *MblRNAi*-induced conduction defects, we performed genetic rescue experiments by attenuating *stj* expression *via* RNAi in *Hand>Bru-3* and *Hand>MblRNAi* flies (**Fig. 4B**). Intriguingly, lowering *stj* transcript levels in the heart was sufficient to rescue asynchronous heartbeat in *Hand>Bru-3* flies but less so in *Hand>MblRNAi* flies where rescue was only partial (**Fig. 4B**). This suggests that a fine-tuning of Ca^{2+} level by *stj/α2δ3* but

potentially also other calcium regulators may be at work to ensure synchronous heart beating and avoid conduction block. Importantly, as recently reported [40], Ca-α1D is the main Ca^{2+} channel operating in the fly heart and is not only required for cardiac contractions but also regulates propagation of calcium waves. This suggests that Stj-driven potentiation of Ca-α1D channel function could lead to accelerated calcium waves in a portion of the heart inducing asynchronous heartbeats. Thus, even if no specialized conduction system is present in the *Drosophila* heart, propagation of calcium waves along the cardiac tube is finely regulated to ensure synchronous heartbeats.

Taken together, with evidence based on heart-specific transcriptional profiling of *Drosophila* models, we propose that the conduction disturbance observed in DM1, linked to an imbalance between RNA-binding factors MBNL1/Mbl and CELF1/Bru-3, arises from likely impacted Ca-α1D/Cav1.2 calcium channel function in cardiomyocytes (scheme, **Fig. 4C**) where *stj/α2δ3* encoding regulatory subunit of cardiac calcium channel plays a central role.

MATERIALS AND METHODS

Drosophila stocks

All fly stocks were maintained at 25°C on standard fly food in a 12h:12h light–dark cycling humidified incubator. To generate the DM1 *Drosophila* models, we used the inducible lines *UAS-MblRNAi* (v28732, VDRC, Vienna, Austria) and *UAS-Bru3 37* (*bru-3*^{d09837}, BDSC, Bloomington, USA) and crossed them with the driver line, *Hand-Gal4* [41,42] (kindly provided by L. Perrin, TAGC, Marseille), to target transgene expression to the adult fly heart (cardiomyocytes and pericardial cells). To examine the expression pattern of the *Hand-Gal4* driver line, we crossed them to *UAS-GFP* line (#32201, BDSC, Bloomington, USA). Control lines were generated by crossing the above-cited lines with w^{1118} flies. For TU-tagging experiments, the UPRT line (*UAS-HA-UPRT* 3.2, #27604, BDSC, Bloomington, USA) was combined with the previously cited UAS lines and with *UAS-LacZ* (#1776, BDSC, Bloomington, USA) as a control, generating *UAS-LacZ;UAS-HA-UPRT*, *UAS-MblRNAi;UAS-HA-UPRT* and *UAS-Bru3;UAS-HA-UPRT* stocks. For functional analyses of *straightjacket*, the lines used were *UAS-Stj* (FlyORF, F 001252) and *UAS-stj RNAi* (#25807, BDSC, Bloomington, USA) and *tin*CΔ4-Gal4 cardiomyocyte-specific driver [43,44] (kindly provided by R. Bodmer, SBPMD Institute, San Diego). For functional analyses of *Ca-a1D* and *Rgk2,* we used #25830 and #65932 RNAi lines (BDSC, Bloomington, USA), respectively. The

UAS-GCaMP3 line (#32116, BDSC, Bloomington, USA) was crossed to *Hand-Gal4* driver and applied as a sensor of calcium waves in the cardiac tube.

Optical heartbeat analyses of adult *Drosophila* hearts

To assess cardiac physiology in adult flies, we used the method previously described [14,23]. Briefly, 1-week old flies were anesthetized using FlyNap (# 173025, Carolina) then dissected in artificial hemolymph solution, removing the head, legs, wings, gut, ovaries and fat body. The hearts were allowed to equilibrate with oxygenation for 15–20 minutes prior to filming 30-second movies with a Hamamatsu camera (Frame rate>100 frames/sec) under a Zeiss microscope (10X magnification). Movie analysis was performed by SOHA (Semi-automatic Optical Heartbeat Analysis) based on using Matlab R2009b (Mathworks, Natick, MA, USA) to collect contractility (diastolic and systolic diameters, fractional shortening) and rhythmicity (heart period, diastolic and systolic intervals and arrhythmicity index) parameters.

RIP with anti-Bru-3 antibody

RIP experiment with anti-Bru-3 antibody or with non-immune rabbit serum as a control was performed on cell lysate from 20 dissected *Hand>Bru-3* fly hearts according to previously described protocol [45]. RNA isolated from the immunoprecipitated material was reverse transcribed and used for PCR detection to test for the presence of 3'UTR *stj* sequences containing potential Bru-3 binding sites. 35 cycles of PCR amplification (95°C 1min, 62°C, 1min and 72°C, 2min) was used with the following pair of primers: F-stj CTTAAACGACTTGCAACCTTC and R-stj GGTTAAACGTACTTCCGATTC

Immunofluorescence on *Drosophila* heart

Briefly, the fly hearts were dissected as described above and fixed for 15 minutes in 4% formaldehyde. The immunostaining procedure was performed as previously [13]. The following primary antibodies were used: sheep anti-Mbl antibody (kindly provided by Darren Monckton), rabbit anti-Bru-3 (1:1000; Millegen, Toulouse, France), rabbit anti-Stj (1:500; kindly provided by Greg Neely) and goat anti-GFP (1:500, Abcam, ab 5450). Rhodamine phalloidin (ThermoFischer Scientific) was used to reveal actin filaments. Fluorescent secondary antibodies were from Jackson ImmunoResearch. For Mbl, we used a biotinylated anti-sheep antibody (Biotin-SP-AffiniPure Donkey Anti-Sheep IgG (H+L), Jackson ImmunoResearch) combined with a DTAF-Conjugated Streptavidin (Jackson ImmunoResearch).

RNA extraction and RT-qPCR on adult fly heart samples

Total RNA was isolated from about 10-15 hearts from 1-week old flies, using TRIzol reagent (Invitrogen) combined to the Quick-RNA MicroPrep Kit (Zymo Research) following manufacturer's instructions. RNA quality and quantity were respectively assessed using Agilent RNA 6000 Pico kit on Agilent 2100 Bioanalyzer (Agilent Technologies) and Qubit RNA HS assay kit on Qubit 3.0 Fluorometer (Thermo Fischer Scientific). RT-qPCR was performed as previously described [13], using *Rp49* as a reference gene.

Immunofluorescence on murine heart

Mouse hearts were dissected and fixed for 2h in paraformaldehyde (4% in 1X PBS) at 4°C and processed for cryosectioning as described elsewhere [46]. Frozen sections were incubated overnight at 4°C with anti-α2δ3 (1:200) [38]. Fluorescent images were obtained using a Zeiss AxioimagerZ1 with an Apotome module and an AxioCamMRm camera.

RNA extraction and RT-qPCR on murine heart samples

RNA extraction was performed as described elsewhere [39]. Transcripts were amplified in a 7300 real-time PCR system (Applied Biosystems) using Power SybrGreen detection (Life Technologies). Standard curves were established with mouse tissues expressing the tested genes. Samples were quantified in triplicate, and experiments were repeated twice. *Cac2d3* transcripts were amplified using forward primer GGGAACCAGATGAGAATGGAGTC and reverse primer TTTGGAGAAGTCGCTGCCTG. *Polr2a* was used as internal control (forward primer GGCTGTGCGGAAGGCTCTG and reverse primer TGTCCTGGCGGTTGACCC).

RNA extraction and RT-qPCR on DM1 patient cardiomyocytes

Human ventricular cardiac muscle tissues were obtained at autopsy from 5 DM1 patients and 4 normal controls. Total mRNA was extracted and first-strand complementary DNA synthesized using protocols described previously [47]. RT-qPCR was performed using TaqMan Gene Expression assays (Hs01045030_m1 and 4333760F, Applied Biosystems) on an ABI PRISM 7900HT Sequence Detection System (Applied Biosystems), as described previously [48]. Level of CACNA2D3/*α2δ3* mRNA was normalized to 18S rRNA.

TU-tagging experiments

The TU-tagging protocol was adapted from previously published studies [18,49].

4TU treatment, fly collection, and total RNA extraction

TU-tagging experiments were performed on the following 1-week-old adult flies: *Hand>LacZ;HA-UPRT*, *Hand>MblRNAi;HA-UPRT* and *Hand>Bru3;HA-UPRT*. Briefly, flies were starved for 6 hours at 25°C and transferred to fresh food media containing 4TU (Sigma) at 1 mM. After a 12-hour incubation at 29°C, about 30 to 40 flies of the described genotypes were dissected (removing the head, wings, legs, ovaries and gut) in DPBS 1X (Gibco, Life Technologies), immediately transferred to Eppendorf tubes, and snap-frozen in liquid nitrogen. Total RNA isolation was performed as described above in TRIzol following the manufacturer's instructions (ThermoFischer Scientific).

Purification of TU-tagged RNA

Bio-thio coupling was performed on about 30 µg of total RNA with 1 mg/mL biotin-HPDP (Pierce) for three hours followed by two chloroform purification steps to eliminate the unbound biotin, as previously described [18]. To verify the efficiency of the biotinylation step, a RNA dot blot was performed using streptavidin-HRP antibody. Next, the streptavidin purification step served to collect the thiolated-RNA fraction (cardiac-specific 4TU) and the unbound fraction (non-cardiac RNAs) using a µMACS Streptavidin kit (MACS, Miltenyi Biotec) following the manufacturer's instructions. The purified fraction was precipitated as previously described [18]. RNA quality and quantity were assessed using Bioanalyzer and Qubit systems according to the manufacturer's instructions. RT-qPCR was performed to check for enrichment of cardiac-specific transcripts (*Hand* and *H15*) by comparing 4TU fraction relative to input fraction (i.e. the biotinylated fraction containing cardiac and non-cardiac RNAs), with *Rp49* gene used as reference.

RNA sequencing

Library preparation

Library preparation was performed on about 50 ng of cardiac-specific RNA from the previously described conditions, using the Ovation RNA-Seq Systems 1-16 for Model Organisms adapted to *Drosophila* (NuGEN, #0350-32) as per the manufacturer's instructions with a few modifications. First-strand synthesis was performed with the integrated DNAse treatment (HL-dsDNAse, ArcticZymes) and cDNA was fragmented using a Bioruptor sonication system (Diagenode) via 30 cycles of 30 seconds ON/OFF on low power. 15 PCR library amplification cycles were performed on 50 ng of starting RNA, and a size-selective bead purification step was done using RNAClean XP beads (Agencourt AMPure, Beckman

Coulter). Quantitative and qualitative assessment of the library was performed using an Agilent dsDNA HS kit on an Agilent 2100 Bioanalyzer (Agilent Technologies).

Sequencing parameters

The indexed Illumina libraries prepared from the cardiac-specific *Hand>LacZ;HA-UPRT, Hand>MblRNAi;HA-UPRT* and *Hand>Bru3;HA-UPRT* RNA fractions were mixed at equal concentrations and sequenced (100-bp paired-end reads) on the same lane of a HiSeq 2000 (EMBL Gene Core Illumina Sequencing facility, Heidelberg, Germany). All four genotype sets of 1-week-old flies were sequenced in duplicate to give a total of 8 samples sequenced.

Data analysis

The RNA-sequencing data was checked for good quality using the FastQC package (http://www.bioinformatics.babraham.ac.uk/projects/fastqc/). Each sample was aligned to the reference Dmel genome release 5.49 using Bowtie2 [50]. The aligned reads were sorted and indexed using SAMtools [51]. Pearson correlation was determined for each duplicate of each condition. Differential gene expression was obtained using a pipeline based on the Deseq2 package. Rlog transformation was applied on raw count data obtained for the duplicates of each condition before computing differential expression. Genes were tested individually for differences in expression between conditions. We set a fold-change threshold at 1.7 and p-value threshold at 0.05 for meaningful differential up-expression, and fold-change threshold at 0.59 and p-value threshold at 0.05 for meaningful differential down-expression.

In vivo calcium transient analyses

We performed short (10s) time lapse recording of beating hearts, dissected as for SOHA experiments, and mounted inverted on 35mm glass bottom dishes (IBIDI ref 81218) for imaging on LEICA SP8 confocal microscope. Registered two channels films from single optical level (GCaMP-GFP channel representing calcium waves and transmitted light channel representing contractions) were analyzed using Image J. For each film, we first transformed Frames on Image stacks and used “Plot Z axis profile” function to generate graphs.

Statistical analyses and access to RNAseq data

All statistical analyses were performed using GraphPad Prism v5.02 software (GraphPad Inc, USA. All RNAseq data reported here has been deposited with the GEO-NCBI tracking system under accession number #18843071.

Acknowledgements

This work was supported by AFM-Téléthon (MyoNeurAlp Strategic Program), Agence Nationale de la Recherche (Tefor Infrastructure Grant) and Fondation pour la Recherche Médicale (Equipe FRM Award).

REFERENCES

1. Theadom A, Rodrigues M, Roxburgh R, Balalla S, Higgins C, Bhattacharjee R, Jones K, Krishnamurthi R, Feigin V (2014) Prevalence of Muscular Dystrophies: A Systematic Literature Review. *Neuroepidemiology* **43**: 259–268.
2. Taneja (1995) Foci of trinucleotide repeat transcripts in nuclei of myotonic dystrophy cells and tissues. *J Cell Biol* **128**: 995–1002.
3. Davis BM, McCurrach ME, Taneja KL, Singer RH, Housman DE (1997) Expansion of a CUG trinucleotide repeat in the 3′ untranslated region of myotonic dystrophy protein kinase transcripts results in nuclear retention of transcripts. *Proc Natl Acad Sci U S A* **94**: 7388–7393.
4. Kuyumcu-Martinez NM, Wang G-S, Cooper TA (2007) Increased steady-state levels of CUGBP1 in myotonic dystrophy 1 are due to PKC-mediated hyperphosphorylation. *Mol Cell* **28**: 68–78.
5. Kino Y, Washizu C, Oma Y, Onishi H, Nezu Y, Sasagawa N, Nukina N, Ishiura S (2009) MBNL and CELF proteins regulate alternative splicing of the skeletal muscle chloride channel CLCN1. *Nucleic Acids Res* **37**: 6477–6490.
6. Savkur RS, Philips AV, Cooper TA (2001) Aberrant regulation of insulin receptor alternative splicing is associated with insulin resistance in myotonic dystrophy. *Nat Genet* **29**: 40–47.
7. Freyermuth F, Rau F, Kokunai Y, Linke T, Sellier C, Nakamori M, Kino Y, Arandel L, Jollet A, Thibault C, et al. (2016) Splicing misregulation of SCN5A contributes to cardiac-conduction delay and heart arrhythmia in myotonic dystrophy. *Nat Commun* **7**: 11067.
8. Sicot G, Gourdon G, Gomes-Pereira M (2011) Myotonic dystrophy, when simple repeats reveal complex pathogenic entities: new findings and future challenges. *Hum Mol Genet* **20**: R116–R123.
9. de Die-Smulders CE, Höweler CJ, Thijs C, Mirandolle JF, Anten HB, Smeets HJ, Chandler KE, Geraedts JP (1998) Age and causes of death in adult-onset myotonic dystrophy. *Brain* **121**: 1557–1563.
10. Mathieu J, Allard P, Potvin L, Prevost C, Begin P (1999) A 10-year study of mortality in a cohort of patients with myotonic dystrophy. *Neurology* **52**: 1658–1658.
11. Groh WJ, Groh MR, Saha C, Kincaid JC, Simmons Z, Ciafaloni E, Pourmand R, Otten RF, Bhakta D, Nair GV, et al. (2008) Electrocardiographic Abnormalities and Sudden Death in Myotonic Dystrophy Type 1. *N Engl J Med* **358**: 2688–2697.
12. Wang G-S, Kuyumcu-Martinez MN, Sarma S, Mathur N, Wehrens XHT, Cooper TA (2009) PKC inhibition ameliorates the cardiac phenotype in a mouse model of myotonic dystrophy type 1. *J Clin Invest* **119**: 3797–3806.
13. Picchio L, Plantie E, Renaud Y, Poovthumkadavil P, Jagla K (2013) Novel Drosophila model of myotonic dystrophy type 1: phenotypic characterization and genome-wide view of altered gene expression. *Hum Mol Genet* **22**: 2795–2810.
14. Ocorr K, Reeves NL, Wessells RJ, Fink M, Chen H-SV, Akasaka T, Yasuda S, Metzger JM, Giles W, Posakony JW, et al. (2007) KCNQ potassium channel mutations cause cardiac arrhythmias in Drosophila that mimic the effects of aging. *Proc Natl Acad Sci U S A* **104**: 3943–3948.
15. Taghli-Lamallem O, Plantié E, Jagla K (2016) Drosophila in the Heart of Understanding Cardiac Diseases: Modeling Channelopathies and Cardiomyopathies in the Fruitfly. *J Cardiovasc Dev Dis* **3**: 7.

16. Picchio L, Legagneux V, Deschamps S, Renaud Y, Chauveau S, Paillard L, Jagla K (2018) Bruno-3 regulates sarcomere components expression and contributes to muscle phenotypes of Myotonic dystrophy type 1. *Dis Model Mech* dmm.031849.
17. Birse RT, Choi J, Reardon K, Rodriguez J, Graham S, Diop S, Ocorr K, Bodmer R, Oldham S (2010) High-fat-diet-induced obesity and heart dysfunction are regulated by the TOR pathway in Drosophila. *Cell Metab* **12**: 533–544.
18. Miller MR, Robinson KJ, Cleary MD, Doe CQ (2009) TU-tagging: cell type–specific RNA isolation from intact complex tissues. *Nat Methods* **6**: 439–441.
19. Dolphin AC (2013) The α2δ subunits of voltage-gated calcium channels. *Biochim Biophys Acta BBA - Biomembr* **1828**: 1541–1549.
20. Hoppa MB, Lana B, Margas W, Dolphin AC, Ryan TA (2012) alpha2delta expression sets presynaptic calcium channel abundance and release probability. *Nature* **486**: 122–125.
21. Mesirca P, Torrente AG, Mangoni ME (2015) Functional role of voltage gated Ca2+ channels in heart automaticity. *Front Physiol* **6**:.
22. Bodi I, Mikala G, Koch SE, Akhter SA, Schwartz A (2005) The L-type calcium channel in the heart: the beat goes on. *J Clin Invest* **115**: 3306–3317.
23. Fink M, Callol-Massot C, Chu A, Ruiz-Lozano P, Belmonte J, Giles W, Bodmer R, Ocorr K (2009) A new method for detection and quantification of heartbeat parameters in Drosophila, zebrafish, and embryonic mouse hearts. *BioTechniques* **46**: 101–113.
24. Voght SP, Fluegel ML, Andrews LA, Pallanck LJ (2007) Drosophila NPC1b Promotes an Early Step in Sterol Absorption from the Midgut Epithelium. *Cell Metab* **5**: 195–205.
25. Galindo K, Smith DP (2001) A large family of divergent Drosophila odorant-binding proteins expressed in gustatory and olfactory sensilla. *Genetics* **159**: 1059–1072.
26. Weerd JH van, Christoffels VM (2016) The formation and function of the cardiac conduction system. *Development* **143**: 197–210.
27. Ueda K, Valdivia C, Medeiros-Domingo A, Tester DJ, Vatta M, Farrugia G, Ackerman MJ, Makielski JC (2008) Syntrophin mutation associated with long QT syndrome through activation of the nNOS-SCN5A macromolecular complex. *Proc Natl Acad Sci U S A* **105**: 9355–9360.
28. Shieh B-H, Zhu M-Y (1996) Regulation of the TRP Ca2+ Channel by INAD in Drosophila Photoreceptors. *Neuron* **16**: 991–998.
29. Spassova MA, Soboloff J, He L-P, Hewavitharana T, Xu W, Venkatachalam K, van Rossum DB, Patterson RL, Gill DL (2004) Calcium entry mediated by SOCs and TRP channels: variations and enigma. *Biochim Biophys Acta BBA - Mol Cell Res* **1742**: 9–20.
30. Su Z, Barker DS, Csutora P, Chang T, Shoemaker RL, Marchase RB, Blalock JE (2003) Regulation of Ca2+ release-activated Ca2+channels by INAD and Ca2+ influx factor. *Am J Physiol-Cell Physiol* **284**: C497–C505.
31. Puhl HL, Lu VB, Won Y-J, Sasson Y, Hirsch JA, Ono F, Ikeda SR (2014) Ancient Origins of RGK Protein Function: Modulation of Voltage-Gated Calcium Channels Preceded the Protostome and Deuterostome Split. *PLoS ONE* **9**:.
32. Magyar J, Kiper CE, Sievert G, Cai W, Shi G-X, Crump SM, Li L, Niederer S, Smith N, Andres DA, et al. (2012) Rem-GTPase regulates cardiac myocyte L-type calcium current. *Channels* **6**: 166–173.
33. Splawski I, Timothy KW, Sharpe LM, Decher N, Kumar P, Bloise R, Napolitano C, Schwartz PJ, Joseph RM, Condouris K, et al. (2004) CaV1.2 Calcium Channel Dysfunction Causes a Multisystem Disorder Including Arrhythmia and Autism. *Cell* **119**: 19–31.

34. Rau F, Freyermuth F, Fugier C, Villemin J-P, Fischer M-C, Jost B, Dembele D, Gourdon G, Nicole A, Duboc D, et al. (2011) Misregulation of miR-1 processing is associated with heart defects in myotonic dystrophy. *Nat Struct Mol Biol* **18**: 840–845.
35. Limpitikul WB, Viswanathan MC, O'Rourke B, Yue DT, Cammarato A (2018) Conservation of cardiac L-type Ca 2+ channels and their regulation in Drosophila : A novel genetically-pliable channelopathic model. *J Mol Cell Cardiol* **119**: 64–74.
36. Weeke P, Muhammad R, Delaney JT, Shaffer C, Mosley JD, Blair M, Short L, Stubblefield T, Roden DM, Darbar D, et al. (2014) Whole-exome sequencing in familial atrial fibrillation. *Eur Heart J* **35**: 2477–2483.
37. Rotstein B, Paululat A (2016) On the Morphology of the Drosophila Heart. *J Cardiovasc Dev Dis* **3**: 15.
38. Neely GG, Hess A, Costigan M, Keene AC, Goulas S, Langeslag M, Griffin RS, Belfer I, Dai F, Smith SB, et al. (2010) A Genome-wide Drosophila Screen for Heat Nociception Identifies α2δ3 as an Evolutionarily Conserved Pain Gene. *Cell* **143**: 628–638.
39. Huguet A, Medja F, Nicole A, Vignaud A, Guiraud-Dogan C, Ferry A, Decostre V, Hogrel J-Y, Metzger F, Hoeflich A, et al. (2012) Molecular, Physiological, and Motor Performance Defects in DMSXL Mice Carrying >1,000 CTG Repeats from the Human DM1 Locus. *PLoS Genet* **8**: e1003043.
40. Lam A, Karekar P, Shah K, Hariharan G, Fleyshman M, Kaur H, Singh H, Gururaja Rao S (2018) Drosophila Voltage-Gated Calcium Channel α1-Subunits Regulate Cardiac Function in the Aging Heart. *Sci Rep* **8**:.
41. Han Z, Olson EN (2005) Hand is a direct target of Tinman and GATA factors during Drosophila cardiogenesis and hematopoiesis. *Development* **132**: 3525–3536.
42. Sellin J, Albrecht S, Kölsch V, Paululat A (2006) Dynamics of heart differentiation, visualized utilizing heart enhancer elements of the Drosophila melanogaster bHLH transcription factor Hand. *Gene Expr Patterns* **6**: 360–375.
43. Lo PCH, Frasch M (2001) A role for the COUP-TF-related gene seven-up in the diversification of cardioblast identities in the dorsal vessel of Drosophila. *Mech Dev* **104**: 49–60.
44. Perrin L, Monier B, Ponzielli R, Astier M, Semeriva M (2004) Drosophila cardiac tube organogenesis requires multiple phases of Hox activity. *Dev Biol* **272**: 419–431.
45. Kachaev ZM, Gilmutdinov RA, Kopytova DV, Zheludkevich AA, Shidlovskii YV, Kurbidaeva AS (2017) RNA immunoprecipitation technique for <Emphasis Type="Italic">Drosophila melanogaster</Emphasis> S2 cells. *Mol Biol* **51**: 72–79.
46. Beyer S, Kelly RG, Miquerol L (2011) Inducible Cx40-Cre expression in the cardiac conduction system and arterial endothelial cells. *Genes N Y N 2000* **49**: 83–91.
47. Nakamori M, Kimura T, Kubota T, Matsumura T, Sumi H, Fujimura H, Takahashi MP, Sakoda S (2008) Aberrantly spliced -dystrobrevin alters -syntrophin binding in myotonic dystrophy type 1. *Neurology* **70**: 677–685.
48. Nakamori M, Gourdon G, Thornton CA (2011) Stabilization of expanded (CTG)•(CAG) repeats by antisense oligonucleotides. *Mol Ther J Am Soc Gene Ther* **19**: 2222–2227.
49. Gay L, Karfilis KV, Miller MR, Doe CQ, Stankunas K (2014) Applying thiouracil tagging to mouse transcriptome analysis. *Nat Protoc* **9**: 410–420.
50. Langmead B, Salzberg SL (2012) Fast gapped-read alignment with Bowtie 2. *Nat Methods* **9**: 357–359.
51. Li H, Handsaker B, Wysoker A, Fennell T, Ruan J, Homer N, Marth G, Abecasis G, Durbin R, 1000 Genome Project Data Processing Subgroup (2009) The Sequence Alignment/Map format and SAMtools. *Bioinforma Oxf Engl* **25**: 2078–2079.

FIGURE LEGENDS

Figure 1. Cardiac-specific knockdown of MBNL1 ortholog and overexpression of CELF1 counterpart in *Drosophila* leads to asynchronous heartbeats. A) The adult *Drosophila* heart expressing Hand-Gal4-driven GFP (*Hand>GFP*). Note that this Gal4 line drives expression exclusively in the heart. Arrows indicate cardiomyocytes (CM) and pericardial cells (PC) and A2–A5 denote abdominal segments. Scale bar, 150 µm. **B**) Movie and M-modes views illustrating asynchronous heartbeats in *Hand>MblRNAi* flies registered in two adjacent heart segments (A3 and A4). Two-sided arrows indicate heart diameter in diastolic state. **C**) Barplot graph showing percentage of flies with conduction defects in the different genetic contexts tested. Note the higher impact of attenuation of *Mbl* compared to overexpression of *Bru-3*. Below are examples of M-modes illustrating "partial" and "total" heart blocks observed in *Hand>MblRNAi* and *Hand>Bru-3* flies with asynchronous heartbeats.

Figure 2. Cardiac-specific transcriptional profiling using TU-tagging in *Hand>MblRNAi* and *Hand>Bru-3* flies reveals commonly deregulated candidates including *straightjacket.* **A**) Venn diagrams of genes deregulated in *Hand>UPRT;MblRNAi* and in *Hand>UPRT;Bru-3* contexts (FC>1.7) followed by heatmap of commonly deregulated genes and Genemania interaction network of conserved candidates including *stj* and three other genes involved in Ca^{2+} regulation. A scheme presenting the structure of the voltage-gated calcium channel and its regulatory component α2δ3 is included. **B)** IGV tracks showing RNAseq peaks over the *stj* locus in healthy control and pathological contexts. Red boxes highlight *stj-B* and C variants that are specifically enriched in *Hand>MblRNAi* and *Hand>Bru-3* contexts. Note that both these *stj* isoforms are long 3'UTR variants that carry potential Bru-3 (green box) and Mbl (red box) binding sites. **C)** RIP experiment with anti-Bru-3 antibodies on dissected adult hearts from *Hand>Bru-3* flies showing that Bru-3 binds to 3'UTR of *stj* transcripts. **D)** Alignment of Stj and α2δ3 protein domains shows structural conservation. VWA denotes the von Willebrand factor, type A domain.

Figure 3. Increased cardiac expression of *Straightjacket* and its ortholog *α2δ3* are associated with conduction defects in DM1. A) Stj protein is detected at a low level in cardiomyocytes (CM) but at a higher level in the ventral longitudinal muscles (VLMs) that underlie adult heart tube. Stj in VLMs and in heart tube-attaching alary muscles (AMs) marks the network of T-tubules. PC denotes pericardial cells. Scale bars, 50 µm. **B**) In mouse, α2δ3 protein is detected at a high level in atrial cardiac cells and at a low level in ventricles. LV

denotes left ventricle. Scale bars, 100 µm. **C**) Scheme of the adult *Drosophila* heart with representation of Stj expression. **D**) RT-qPCR analysis of mouse *α2δ3* transcripts confirms low expression level in ventricles and high expression level in atria. **E**) Both *Hand-Gal4* (whole heart) and *Tin-Gal4* (cardiomyocytes only) driven overexpression of *Stj* lead to asynchronous heartbeats similar to those observed in *Hand>MblRNAi* and *Hand>Bru-3* contexts. **F**) *α2δ3* expression analysis in human ventricular muscle from normal controls and DM1 patients with conduction defects. Note the statistically relevant increase in *α2δ3* transcript levels in ventricles of DM1 patients ($p = 0.0317$, Mann-Whitney *U* test).

Figure 4. Calcium waves in asynchronous heart and rescue of asynchronous heart beating by lowering Stj. A) In wild type hearts, calcium waves underlie cardiac contractions so that calcium peaks (arrows) align with the onset of contractions (arrowheads) in both A3 and A4 segments. In contrast, in asynchronously beating *Hand>MblRNAi* heart, in the anterior A3 segment, calcium peaks (arrows) are not always in perfect alignment with contractions (arrowheads) and could not be detected in A4 segment that does not beat. Notice that GFP signal in Hand>MblRNAi;GCaMP context is lower than in the control (Hand>GCaMP) most probably because of a lower Hand-Gal4 induction in two UAS transgene context. **B)** Barplot representing percentage of flies displaying asynchronous heartbeats in *stj* rescue conditions. **C**) Cartoon illustrating potential Stj/α2δ3 function in cardiac conduction in normal and in DM1 condition. In the *Drosophila* heart, the anteriorly-located pacemaker (red ring) provides excitation signals, which need to be efficiently transmitted posteriorly through the cardiac cells to ensure synchronous contraction of all heart segments and directional pumping of the hemolymph (blue arrows). Excitation-contraction coupling depends on Ca^{2+} inward current, which needs to be finely tuned to allow rapid depolarization-repolarization of cardiomyocytes so that they are ready for next excitation-contraction cycle. The Ca^{2+} entry is regulated by Stj/α2δ3, which when increased (DM1 condition) modifies $Ca_v1.2/\alpha1$ channel opening and leads to a higher Ca^{2+} entry. This puts the depolarization-repolarization timing of cardiomyocytes out of sync with the time-cycle of pacemaker firing, which results in asynchronous heartbeat (conduction defects), ultimately leading to heart block.

Figure 1

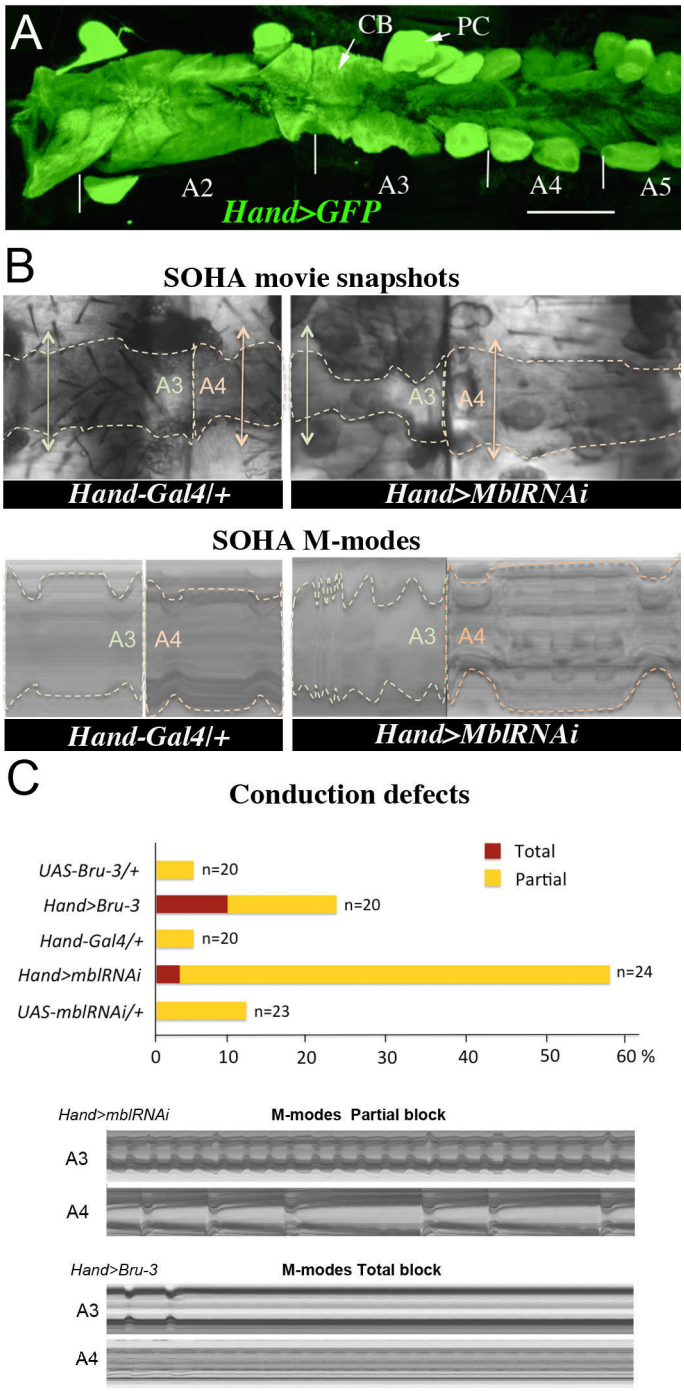
A
CB
PC
A2
A3
A4
A5
Hand>GFP
B
SOHA movie snapshots
A3
A4
Hand-Gal4/+
Hand>MblRNAi
SOHA M-modes
A3
A4
Hand-Gal4/+
Hand>MblRNAi
C
Conduction defects
Total
Partial
UAS-Bru-3/+
Hand>Bru-3
Hand-Gal4/+
Hand>mblRNAi
UAS-mblRNAi/+
n=20
n=20
n=20
n=24
n=23
0
10
20
30
40
50
60 %
Hand>mblRNAi
M-modes Partial block
A3
A4
Hand>Bru-3
M-modes Total block
A3
A4

Figure 2

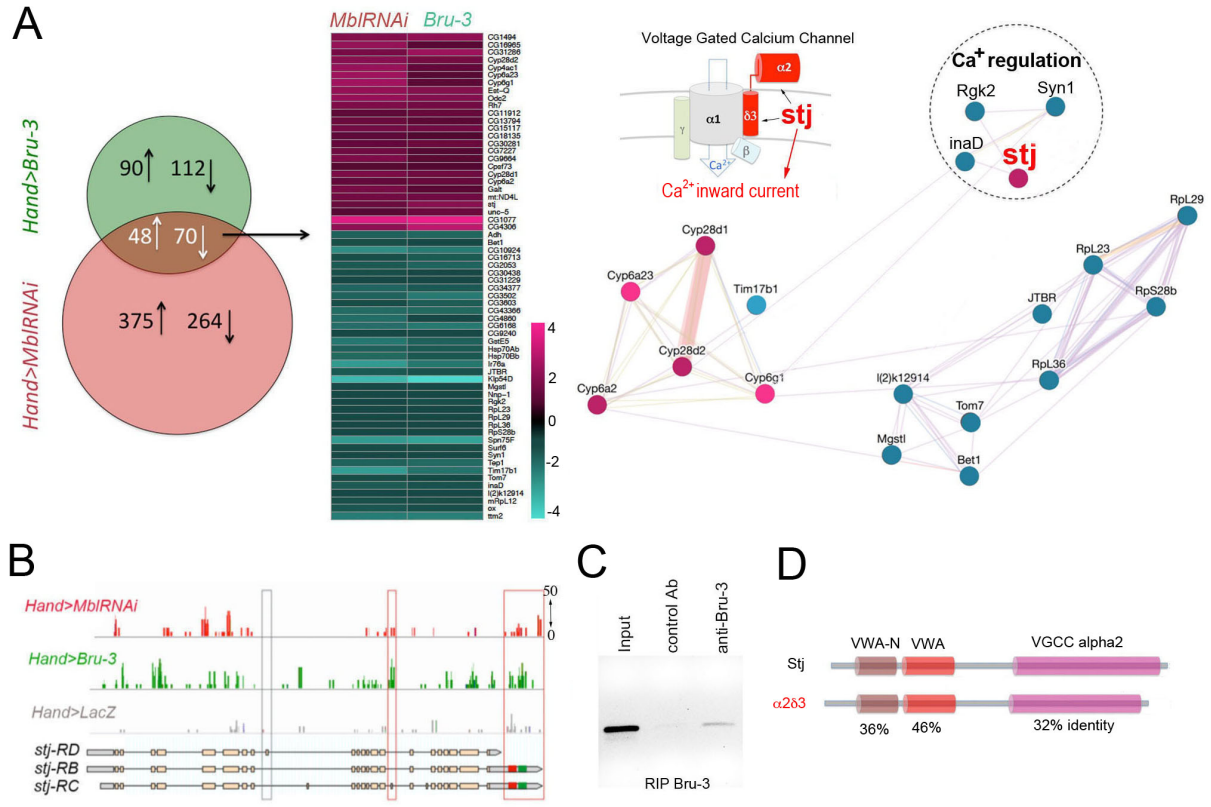
A
Hand>Bru-3
Hand>MblRNAi
90
112
48
70
375
264
MblRNAi
Bru-3
4
2
0
-2
-4
Voltage Gated Calcium Channel
α2
α1
δ3
stj
γ
β
Ca2+
Ca2+ inward current
Ca+ regulation
Rgk2
Syn1
inaD
stj
Cyp28d1
Cyp6a23
Tim17b1
Cyp28d2
Cyp6g1
Cyp6a2
RpL29
RpL23
RpS28b
JTBR
RpL36
l(2)k12914
Tom7
Mgstl
Bet1
B
Hand>MblRNAi
Hand>Bru-3
Hand>LacZ
stj-RD
stj-RB
stj-RC
50
0
C
Input
control Ab
anti-Bru-3
RIP Bru-3
D
Stj
α2δ3
VWA-N
VWA
VGCC alpha2
36%
46%
32% identity

Figure 3

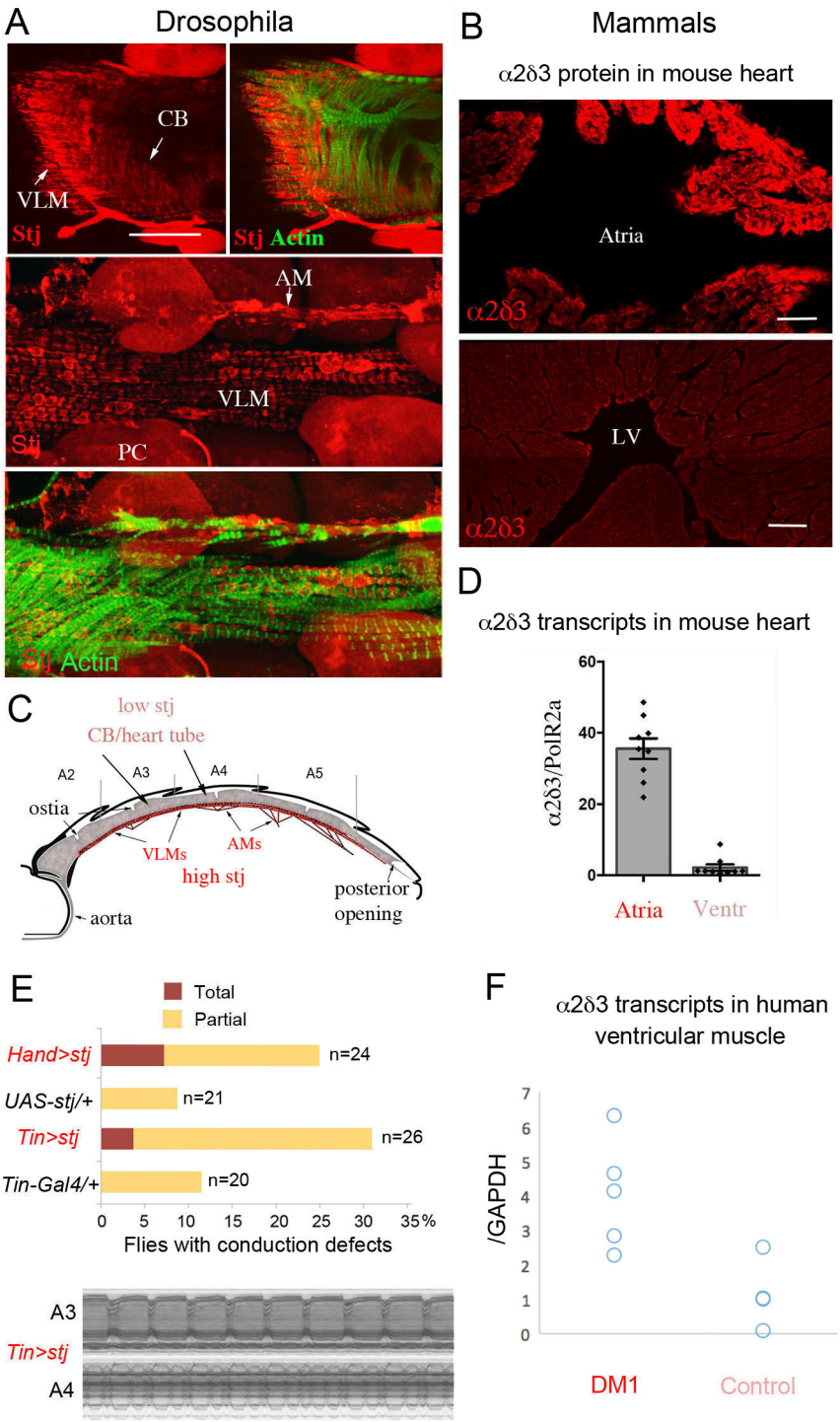
A
Drosophila
CB
VLM
Stj
Stj Actin
AM
VLM
Stj
PC
Stj Actin
B
Mammals
α2δ3 protein in mouse heart
Atria
α2δ3
LV
α2δ3
C
low stj
CB/heart tube
A2
A3
A4
A5
ostia
VLMs
AMs
high stj
posterior opening
aorta
D
α2δ3 transcripts in mouse heart
α2δ3/PolR2a
60
40
20
0
Atria
Ventr
E
Total
Partial
Hand>stj
n=24
UAS-stj/+
n=21
Tin>stj
n=26
Tin-Gal4/+
n=20
0 5 10 15 20 25 30 35%
Flies with conduction defects
A3
Tin>stj
A4
F
α2δ3 transcripts in human ventricular muscle
/GAPDH
7
6
5
4
3
2
1
0
DM1
Control

Figure 4

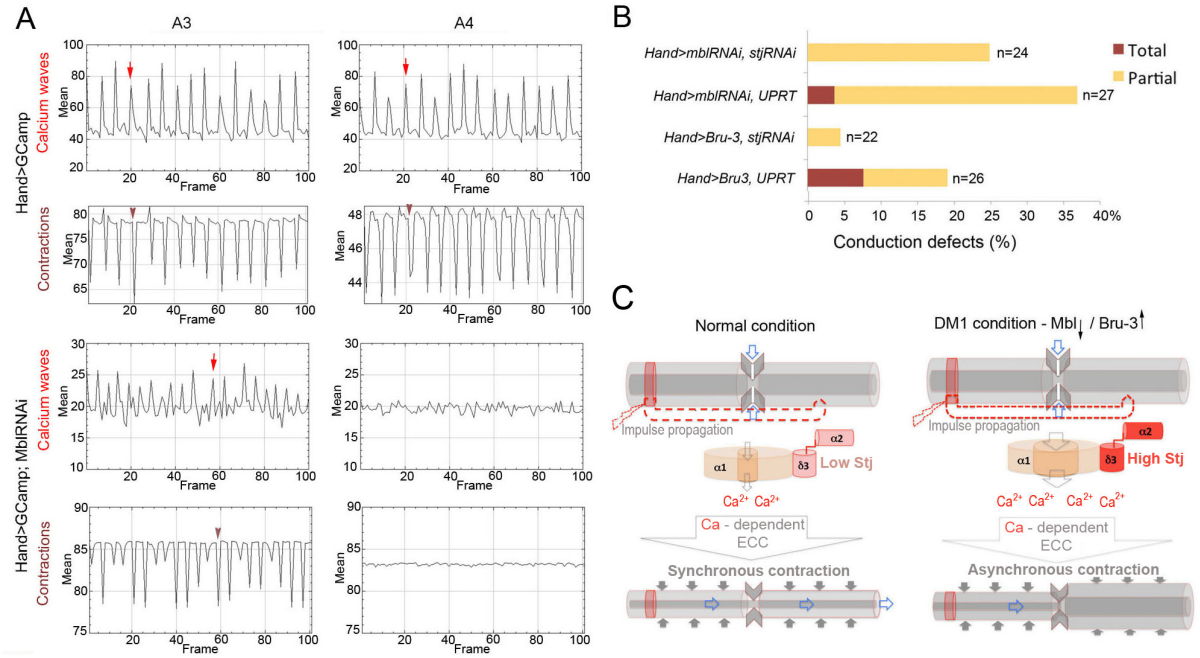
A
A3
A4
Hand>GCamp
Calcium waves
Contractions
Hand>GCamp; MblRNAi
Mean
Frame
B
Hand>mblRNAi, stjRNAi
Hand>mblRNAi, UPRT
Hand>Bru-3, stjRNAi
Hand>Bru3, UPRT
n=24
n=27
n=22
n=26
Total
Partial
Conduction defects (%)
C
Normal condition
DM1 condition - Mbl / Bru-3
Impulse propagation
Low Stj
High Stj
Ca - dependent ECC
Synchronous contraction
Asynchronous contraction

Supplemental information

Table S1. *Drosophila* genes and their Human orthologs deregulated in both *Hand>Bru-3* and *Hand>mblRNAi* contexts.

Fly GeneID	FlyBaseID	Human Symbol	DIOPT Score	Rank	Best Score
Adh	FBgn0000055	HPGD	6	moderate	Yes
Bet1	FBgn0260857	BET1	10	high	Yes
Bet1	FBgn0260857	BET1L	2	moderate	No
CG1077	FBgn0037405	SPINK5	1	low	Yes
CG1077	FBgn0037405	SPINK6	1	low	Yes
CG10924	FBgn0034356	PCK2	11	high	Yes
CG10924	FBgn0034356	PCK1	10	moderate	No
CG11912	FBgn0031248	CTRB2	1	low	Yes
CG11912	FBgn0031248	CTRB1	1	low	Yes
CG11912	FBgn0031248	PRSS38	1	low	Yes
CG11912	FBgn0031248	CTRL	1	low	Yes
CG11912	FBgn0031248	AZU1	1	low	Yes
CG11912	FBgn0031248	PRTN3	1	low	Yes
CG13794	FBgn0031936	SLC6A7	1	low	Yes
CG13794	FBgn0031936	SLC6A14	1	low	Yes
CG1494	FBgn0031169	ABCA3	2	moderate	Yes
CG15117	FBgn0034417	GUSB	12	high	Yes
CG16713	FBgn0031560	WFIKKN1	2	high	Yes
CG16713	FBgn0031560	WFIKKN2	2	high	Yes
CG16713	FBgn0031560	EPPIN-WFDC6	2	moderate	Yes
CG16965	FBgn0032387	PGGHG	10	high	Yes
CG18135	FBgn0036837	GPCPD1	7	moderate	Yes
CG2053	FBgn0039887	CNOT9	3	moderate	Yes
CG30281	FBgn0050281	FIBCD1	4	moderate	Yes
CG30281	FBgn0050281	ANGPTL3	3	moderate	No
CG30281	FBgn0050281	ANGPT4	3	moderate	No
CG30281	FBgn0050281	FGA	3	moderate	No
CG30281	FBgn0050281	ANGPT1	3	low	No
CG30281	FBgn0050281	ANGPT2	3	moderate	No
CG30281	FBgn0050281	FGL2	3	moderate	No
CG30281	FBgn0050281	FCN3	3	low	No
CG30281	FBgn0050281	FCN2	3	low	No
CG30281	FBgn0050281	MFAP4	2	moderate	No
CG30281	FBgn0050281	FCN1	2	low	No
CG30281	FBgn0050281	TNR	2	low	No
CG30281	FBgn0050281	ANGPTL5	2	low	No
CG30281	FBgn0050281	ANGPTL1	2	moderate	No
CG30281	FBgn0050281	TNXB	2	low	No
CG30281	FBgn0050281	FGG	2	low	No
CG30281	FBgn0050281	TNC	2	low	No
CG30281	FBgn0050281	ANGPTL4	2	low	No
CG30281	FBgn0050281	ANGPTL2	2	low	No
CG30281	FBgn0050281	FGB	2	low	No
CG30281	FBgn0050281	TNN	2	low	No
CG30281	FBgn0050281	ANGPTL6	2	low	No

CG30281	FBgn0050281	ANGPTL7	2	low	No
CG30281	FBgn0050281	FGL1	2	low	No
CG30438	FBgn0050438	UGT8	8	high	Yes
CG30438	FBgn0050438	UGT2B10	4	moderate	No
CG30438	FBgn0050438	UGT2B28	3	low	No
CG30438	FBgn0050438	UGT1A3	3	low	No
CG30438	FBgn0050438	UGT3A1	3	low	No
CG30438	FBgn0050438	UGT3A2	3	low	No
CG30438	FBgn0050438	UGT2B4	3	low	No
CG30438	FBgn0050438	UGT2B15	3	low	No
CG30438	FBgn0050438	UGT2A2	3	low	No
CG30438	FBgn0050438	UGT2B17	3	low	No
CG30438	FBgn0050438	UGT2B11	3	low	No
CG30438	FBgn0050438	UGT2A3	3	low	No
CG30438	FBgn0050438	UGT2B7	3	low	No
CG30438	FBgn0050438	UGT1A1	2	low	No
CG31229	FBgn0051229	TIMM22	11	high	Yes
CG31286	FBgn0051286	GLIPR2	3	moderate	Yes
CG31286	FBgn0051286	PI16	2	low	No
CG34377	FBgn0263117	SAMD5	5	high	Yes
CG34377	FBgn0263117	SAMSN1	3	low	No
CG34377	FBgn0263117	SASH3	2	low	No
CG3502	FBgn0046253	LVRN	5	high	Yes
CG3502	FBgn0046253	TRHDE	4	moderate	No
CG3502	FBgn0046253	ANPEP	4	moderate	No
CG3502	FBgn0046253	ENPEP	3	low	No
CG3502	FBgn0046253	LNPEP	3	low	No
CG3502	FBgn0046253	ERAP1	3	low	No
CG3502	FBgn0046253	ERAP2	3	low	No
CG3502	FBgn0046253	NPEPPS	2	low	No
CG3603	FBgn0029648	HSD17B8	11	high	Yes
CG3603	FBgn0029648	CBR4	4	moderate	No
CG4306	FBgn0036787	GGCT	11	high	Yes
CG43366	FBgn0263109	SERPINA5	1	low	Yes
CG43366	FBgn0263109	SERPINA11	1	low	Yes
CG43366	FBgn0263109	SERPINA7	1	low	Yes
CG43366	FBgn0263109	SERPINA1	1	low	Yes
CG43366	FBgn0263109	SERPINA12	1	low	Yes
CG43366	FBgn0263109	SERPINA3	1	low	Yes
CG43366	FBgn0263109	SERPINA13P	1	low	Yes
CG43366	FBgn0263109	SERPINA4	1	low	Yes
CG43366	FBgn0263109	SERPINA2	1	low	Yes
CG43366	FBgn0263109	SERPINA9	1	low	Yes
CG43366	FBgn0263109	SERPINA6	1	low	Yes
CG4860	FBgn0037999	ACADS	7	moderate	Yes
CG4860	FBgn0037999	ACADSB	4	moderate	No

CG6168	FBgn0036154	QPCT	6	moderate	Yes
CG6168	FBgn0036154	QPCTL	5	moderate	No
CG7227	FBgn0031970	CD36	3	moderate	Yes
CG7227	FBgn0031970	SCARB1	3	moderate	Yes
CG7227	FBgn0031970	SCARB2	2	low	No
CG9240	FBgn0030669	IMMP1L	11	high	Yes
CG9664	FBgn0031515	ABCG1	5	moderate	Yes
CG9664	FBgn0031515	ABCG4	4	moderate	No
CG9664	FBgn0031515	ABCG8	2	low	No
Cpsf73	FBgn0261065	CPSF3	11	high	Yes
Cyp28d1	FBgn0031689	TBXAS1	4	moderate	Yes
Cyp28d1	FBgn0031689	CYP3A43	3	low	No
Cyp28d1	FBgn0031689	CYP3A4	3	low	No
Cyp28d1	FBgn0031689	CYP3A5	3	low	No
Cyp28d1	FBgn0031689	CYP3A7-CYP3A51	2	low	No
Cyp28d2	FBgn0031688	TBXAS1	4	moderate	Yes
Cyp28d2	FBgn0031688	CYP3A43	3	low	No
Cyp28d2	FBgn0031688	CYP3A4	3	low	No
Cyp28d2	FBgn0031688	CYP3A5	3	low	No
Cyp28d2	FBgn0031688	CYP3A7-CYP3A51	2	low	No
Cyp4ac1	FBgn0031693	CYP4V2	4	moderate	Yes
Cyp4ac1	FBgn0031693	CYP4A11	3	low	No
Cyp4ac1	FBgn0031693	CYP4Z1	3	low	No
Cyp4ac1	FBgn0031693	CYP4B1	3	low	No
Cyp4ac1	FBgn0031693	CYP4F11	3	moderate	No
Cyp4ac1	FBgn0031693	CYP4X1	3	low	No
Cyp4ac1	FBgn0031693	CYP4F12	3	low	No
Cyp4ac1	FBgn0031693	CYP4A22	3	low	No
Cyp4ac1	FBgn0031693	CYP4F8	2	moderate	No
Cyp4ac1	FBgn0031693	CYP19A1	2	moderate	No
Cyp4ac1	FBgn0031693	CYP4F3	2	low	No
Cyp4ac1	FBgn0031693	CYP4F2	2	low	No
Cyp4ac1	FBgn0031693	CYP4F22	2	moderate	No
Cyp6a2	FBgn0000473	TBXAS1	6	moderate	Yes
Cyp6a2	FBgn0000473	CYP3A43	4	moderate	No
Cyp6a2	FBgn0000473	CYP3A4	4	moderate	No
Cyp6a2	FBgn0000473	CYP3A5	4	moderate	No
Cyp6a2	FBgn0000473	CYP3A7-CYP3A51	2	low	No
Cyp6a2	FBgn0000473	CYP3A7	2	low	No
Cyp6a23	FBgn0033978	TBXAS1	6	moderate	Yes
Cyp6a23	FBgn0033978	CYP3A4	5	moderate	No
Cyp6a23	FBgn0033978	CYP3A43	4	moderate	No
Cyp6a23	FBgn0033978	CYP3A5	4	moderate	No
Cyp6a23	FBgn0033978	CYP3A7-CYP3A51	2	low	No
Cyp6a23	FBgn0033978	CYP3A7	2	low	No
Cyp6g1	FBgn0025454	TBXAS1	4	moderate	Yes

Cyp6g1	FBgn0025454	CYP3A43	3	low	No
Cyp6g1	FBgn0025454	CYP3A4	3	low	No
Cyp6g1	FBgn0025454	CYP3A5	3	low	No
Cyp6g1	FBgn0025454	CYP3A7-CYP3A51	2	low	No
Est-Q	FBgn0037090	CES4A	2	high	Yes
Est-Q	FBgn0037090	CES5A	2	high	Yes
Est-Q	FBgn0037090	CES3	2	high	Yes
Galt	FBgn0263200	GALT	11	high	Yes
GstE5	FBgn0063495	GSTT2B	2	moderate	Yes
GstE5	FBgn0063495	GSTT1	2	moderate	Yes
GstE5	FBgn0063495	GSTT2	2	moderate	Yes
Hsp70Ab	FBgn0013276	HSPA1A	5	high	Yes
Hsp70Ab	FBgn0013276	HSPA1B	5	moderate	Yes
Hsp70Ab	FBgn0013276	HSPA1L	4	moderate	No
Hsp70Ab	FBgn0013276	HSPA6	4	moderate	No
Hsp70Ab	FBgn0013276	HSPA8	3	low	No
Hsp70Ab	FBgn0013276	HSPA2	3	low	No
Hsp70Ab	FBgn0013276	HSPA5	2	low	No
Hsp70Bb	FBgn0013278	HSPA1A	5	high	Yes
Hsp70Bb	FBgn0013278	HSPA1B	5	moderate	Yes
Hsp70Bb	FBgn0013278	HSPA1L	4	moderate	No
Hsp70Bb	FBgn0013278	HSPA6	4	moderate	No
Hsp70Bb	FBgn0013278	HSPA8	3	low	No
Hsp70Bb	FBgn0013278	HSPA2	3	low	No
Hsp70Bb	FBgn0013278	HSPA5	2	low	No
Ir76a	FBgn0260874	GRID2	2	high	Yes
JTBR	FBgn0025820	JTB	9	high	Yes
Klp54D	FBgn0263076	KIF12	10	high	Yes
Mgstl	FBgn0025814	MGST1	10	high	Yes
Mgstl	FBgn0025814	PTGES	4	moderate	No
Nnp-1	FBgn0022069	RRP1	9	high	Yes
Nnp-1	FBgn0022069	RRP1B	8	moderate	No
Odc2	FBgn0013308	ODC1	9	moderate	Yes
Odc2	FBgn0013308	AZIN1	7	moderate	No
Odc2	FBgn0013308	AZIN2	6	moderate	No
Rgk2	FBgn0085419	REM1	7	high	Yes
Rgk2	FBgn0085419	RRAD	6	moderate	No
Rgk2	FBgn0085419	REM2	5	moderate	No
Rgk2	FBgn0085419	GEM	5	moderate	No
Rh7	FBgn0036260	OPN4	3	moderate	Yes
Rh7	FBgn0036260	OPN3	2	moderate	No
Rh7	FBgn0036260	RRH	2	moderate	No
Rh7	FBgn0036260	OPN5	2	moderate	No
RpL23	FBgn0010078	RPL23	10	high	Yes
RpL29	FBgn0016726	RPL29	7	high	Yes
RpL36	FBgn0002579	RPL36	9	high	Yes

RpS28b	FBgn0030136	RPS28	10	high	Yes
Spn75F	FBgn0052203	SERPINA5	1	low	Yes
Spn75F	FBgn0052203	SERPINA11	1	low	Yes
Spn75F	FBgn0052203	SERPINA7	1	low	Yes
Spn75F	FBgn0052203	SERPINA1	1	low	Yes
Spn75F	FBgn0052203	SERPINA12	1	low	Yes
Spn75F	FBgn0052203	SERPINA3	1	low	Yes
Spn75F	FBgn0052203	SERPINA13P	1	low	Yes
Spn75F	FBgn0052203	SERPINA4	1	low	Yes
Spn75F	FBgn0052203	SERPINA2	1	low	Yes
Spn75F	FBgn0052203	SERPINA9	1	low	Yes
Spn75F	FBgn0052203	SERPINA6	1	low	Yes
Spn75F	FBgn0052203	SERPINF2	1	low	Yes
Surf6	FBgn0038746	SURF6	7	high	Yes
Syn1	FBgn0037130	SNTB1	10	high	Yes
Syn1	FBgn0037130	SNTB2	8	moderate	No
Syn1	FBgn0037130	SNTA1	5	moderate	No
Tep1	FBgn0041183	CD109	5	moderate	Yes
Tep1	FBgn0041183	C3	3	low	No
Tep1	FBgn0041183	C4B	3	moderate	No
Tep1	FBgn0041183	C4A	3	low	No
Tep1	FBgn0041183	A2ML1	2	low	No
Tep1	FBgn0041183	C5	2	low	No
Tim17b1	FBgn0037310	TIMM17B	7	moderate	Yes
Tim17b1	FBgn0037310	TIMM17A	7	moderate	Yes
Tom7	FBgn0033357	TOMM7	9	high	Yes
inaD	FBgn0001263	LNX2	3	high	Yes
inaD	FBgn0001263	LNX1	3	high	Yes
inaD	FBgn0001263	MPDZ	2	low	No
inaD	FBgn0001263	PATJ	2	low	No
l(2)k12914	FBgn0263852	DAD1	11	high	Yes
mRpL12	FBgn0011787	MRPL12	9	high	Yes
mRpL12	FBgn0011787	SLC25A10	2	low	No
mt:ND4L	FBgn0013683	ND4L	8	high	Yes
ox	FBgn0011227	UQCR10	8	high	Yes
stj	FBgn0261041	CACNA2D3	11	high	Yes
stj	FBgn0261041	CACNA2D4	9	moderate	No
stj	FBgn0261041	CACNA2D1	2	moderate	No
stj	FBgn0261041	CACNA2D2	2	low	No
ttm2	FBgn0035124	TIMM50	8	moderate	Yes
unc-5	FBgn0034013	UNC5C	11	high	Yes
unc-5	FBgn0034013	UNC5B	9	moderate	No
unc-5	FBgn0034013	UNC5A	8	moderate	No
unc-5	FBgn0034013	UNC5D	7	moderate	No
unc-5	FBgn0034013	UNC5CL	3	moderate	No

Figure S1. Bru-3 and Mbl are expressed in the adult fly heart. **A, A'.** A3 segment of the adult heart. Bru-3 protein is detected in the nuclei of cardiomyocytes (CM), pericardial cells (PC) and ventral longitudinal muscle (VLM). A faint granular cytoplasmic expression could be detected, well seen in PCs. **B**. A similar view of A3 heart segment showing nuclear Mbl accumulation in CMs, PCs and the VLM. Apparent sarcomeric localization of Mbl is detected in circular fibers of CMs and in the VLM. Notice Bru-3 and Mbl expression in nuclei of somatic muscles (sm). Scale bars, 50 μm. **C, D**. RT-qPCR analyses of Mbl attenuation and Bru-3 overexpression in the adult hearts from *Hand>MblRNAi* (C) and *Hand>Bru-3* flies (D). **E-H.** Immunodetection of Mbl and Bru-3 proteins in the hearts of Hand>Bru-3 (E) and *Hand>MblRNAi* flies **G.** Notice homogenous Hand-Gal4-driven overexpression of Bru-3 and homogenous attenuation of Mbl along the heart tube. Scale bars, 100 μm.

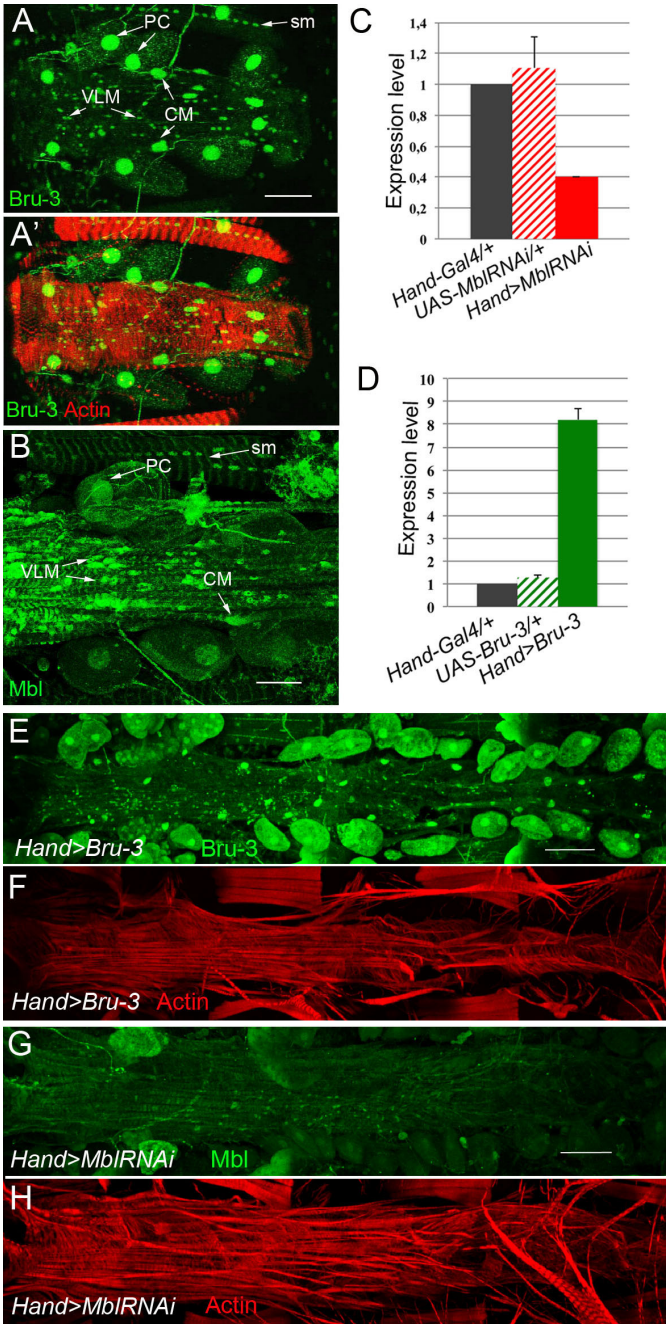

Figure S2. A) Pipeline of heart-targeted transcriptional profiling using TU-tagging. Note that Gal4- inducible UPRT transgene (*UAS-UPRT*) has been combined with *UAS-MblRNAi* and with *UAS-Bru-3* for the purpose of TU-tagging. *Hand>UPRT;lacZ* is the control line used to identify pathogenic gene deregulations in *Hand>UPRT;MblRNAi* and *Hand>UPRT;Bru-3* contexts. Flies were starved at day 4 for 6 hours before being transferred to 4TU containing food for 12 hours. Volcano plot and IGV tracks from control *Hand>UPRT;lacZ* flies show examples of enrichment of heart-specific genes (e.g. *Hand*, *Tin*) (red, right side) and depletion of non-heart-expressed genes (blue, left side), thus validating the specificity of heart targeting. (**B**) *CG42817* and *CG16868* encoding 2 additional *Drosophila* α2δ proteins do not change their expression levels in *Hand>MblRNAi* and in *Hand>Bru-3* contexts. RNAseq IGV tracks in control (*Hand>lacZ*) and in pathogenic DM1 contexts (*Hand>MblRNAi* and *Hand>Bru-3*) are shown aligned with genomic exon/intron organization of both genes.

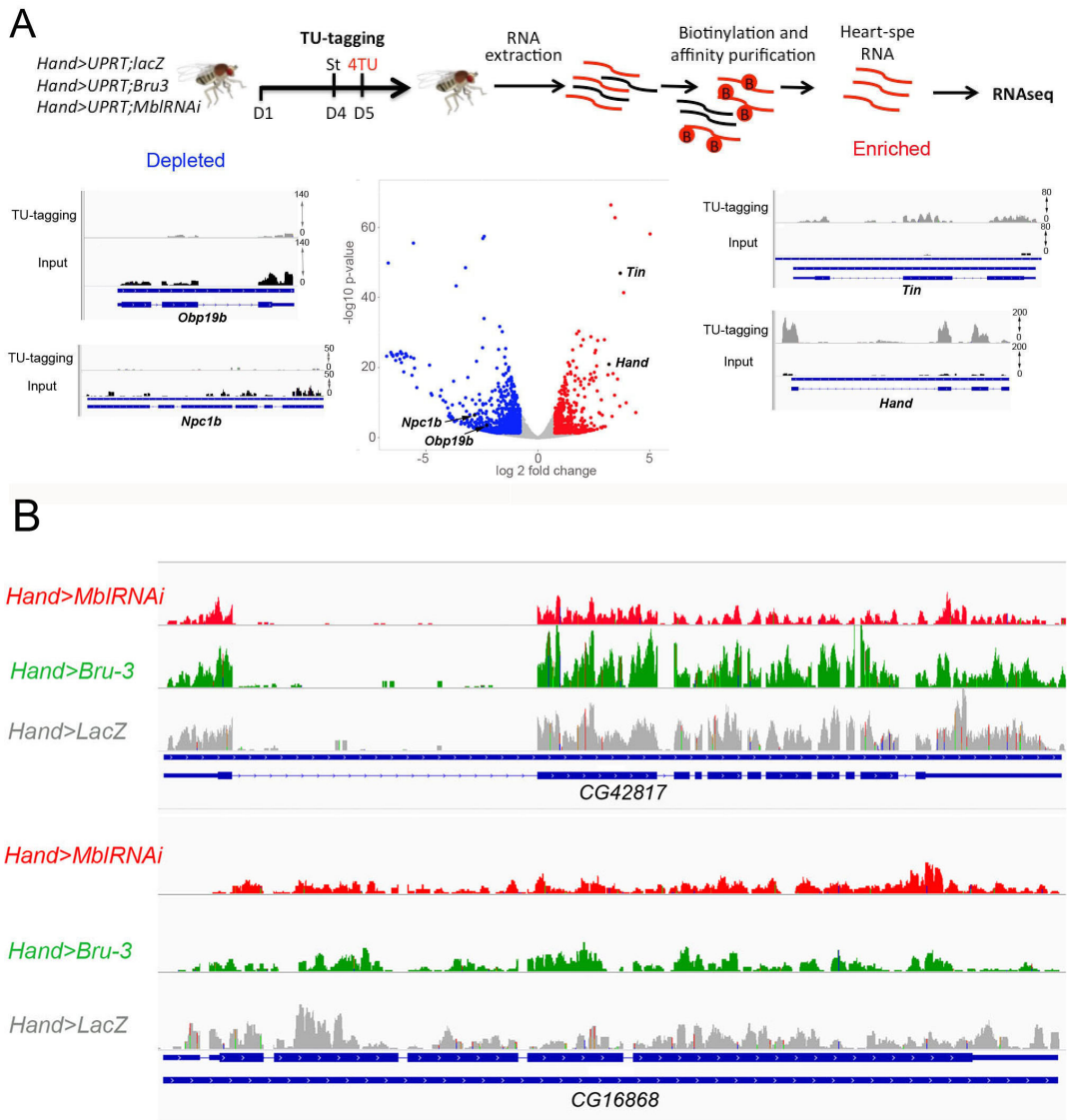

Figure S3. Attenuation of *Ca-α1D* and *Rgk2* affects cardiac function. **A.** IGV RNAseq tracks for *Ca-α1D* transcripts showing reduced transcript levels in *Hand >MblRNAi* context and revealing no Mbl and/or Bru-3 dependent alternative splice regulation of *Ca-α1D*. **B**. Attenuation of *Ca-α1D* and *Rgk2* results in an important number of flies with asystolic hearts. **C**. Attenuation of *Ca-α1D* and *Rgk2* affects contractile (fractional shortening) and rhythmic (arrhythmia index) heart parameters. **D**. Asynchronous heart beating could be detected in *Hand>Ca-α1DRNAi* but not in *Hand>Rgk2RNAi* context.

A

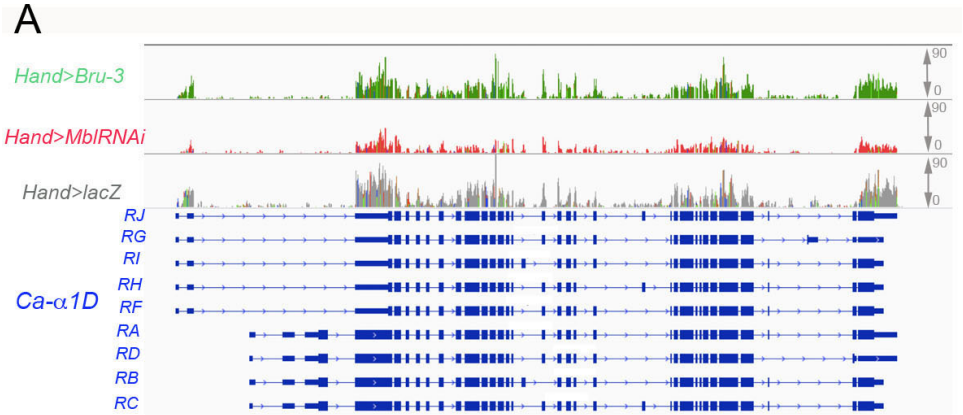

B

Genotype	No flies	No partial asystole	No total asystole	% partial asystole	% total asystole
UAS-Ca-α1DRNAi/+	22	0	1	0	4,5
Hand>Ca-α1DRNAi	22	0	7	0	31,8
UAS-Rgk2RNAi/+	18	1	0	5,6	0
Hand>Rgk2RNAi	22	5	3	22,7	13,6

C

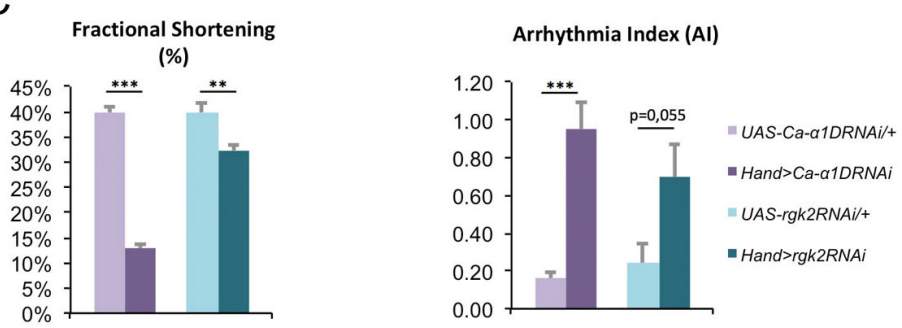

D

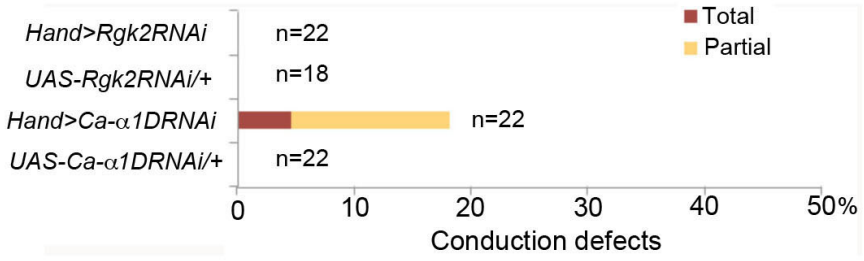

Figure S4. Stj protein expression (red) in circular fibers of cardiomyocytes in wild-type (wt, **A**) and in different genetic contexts (**B-E**) tested. Circular fibers are visualized with phalloidin staining (green). Notice that Stj protein levels appear higher in *Hand>Bru-3* and in *Hand>mblRNAi* compared to wt. High signal level in *Hand>stj* and loss of signal in *Hand>stjRNAi* demonstrate also the specificity of antibodies. Scale bars, 50 μm. **F**. Corrected total cell fluorescence (CTCF) of Stj signal in circular fibers of cardiomyocytes in different genetic contexts measured using Image J according to Burgess et al.,[1].

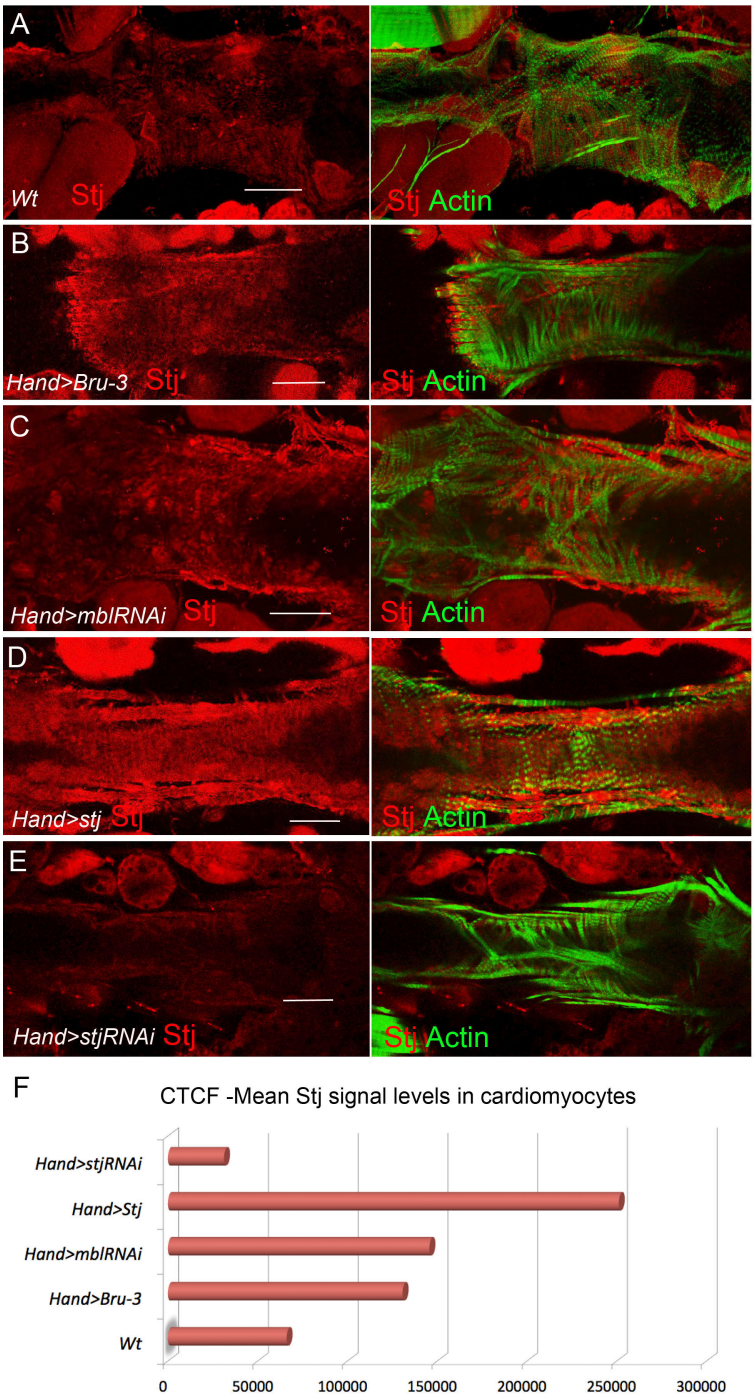

Supplemental reference

1. Burgess A, Vigneron S, Brioudes E, Labbé J-C, Lorca T, Castro A (2010) Loss of human Greatwall results in G2 arrest and multiple mitotic defects due to deregulation of the cyclin B-Cdc2/PP2A balance. *Proc Natl Acad Sci* **107**: 12564–12569.